PAPER • **OPEN ACCESS**

Surface dynamics and electrochemical examination of Co_3O_4 films by iron doping

To cite this article: Emin Yakar *et al* 2024 *Surf. Topogr.: Metrol. Prop.* **12** 035025

Surface Topography: Metrology and Properties

PAPER

Surface dynamics and electrochemical examination of Co_3O_4 films by iron doping

Emin Yakar[1], **Fatma Sarf**[2,*], **Mehmet Bayirli**[3] **and Aykut Ilgaz**[3]

[1] Materials Science and Engineering, Engineering Faculty, Canakkale Onsekiz Mart University, Canakkale, Turkey
[2] Can Vocational School, Canakkale Onsekiz Mart University, Canakkale, Turkey
[3] Physics Department, Balıkesir University, Balıkesir, Turkey
[*] Author to whom any correspondence should be addressed.

E-mail: eyakar@comu.edu.tr, ftm_ozutokk@hotmail.com, mbayirli@balikesir.edu.tr and aykut17ilgaz@gmail.com

Keywords: nanosize, surface fractal analysis, energy storage and conversion

OPEN ACCESS

RECEIVED
16 November 2023

REVISED
1 May 2024

ACCEPTED FOR PUBLICATION
11 June 2024

PUBLISHED
7 August 2024

Abstract

This study focused on Co_3O_4 films, which were prepared by cost-effective chemical bath deposition on In:SnO_2 (ITO) substrates with iron doping concentrations ranging from 2 to 6 mol %. Structural properties were investigated by XRD as well as nanotexture of Fe: Co_3O_4 films was captured via SEM and detailed fractal analysis was analyzed in each prepared film. Effective using of prepared Fe: Co_3O_4 electrodes for electrochemical charge storage applications has been examined by using CV and EIS. From x-ray patterns, spinel cubic structure of Co_3O_4 was observed in all samples, while peaks with Co_2O_3 and substrate indexed peaks were also shown. Pure and iron doped Co_3O_4 surfaces have spherical agglomerative forms while porous structures were observed in 4% Co_3O_4 samples. Redox peaks induced by Faradaic reactions in the CV plots present pseudo- capacitive nature for all electrodes and improves charge transfer process in 4% Co_3O_4 and 6% Co_3O_4 from EIS measurements. Additionally, using scaling theory, the coverage ratio, fractal dimensions, cluster sizes and interface critical exponent values of the superficial hetero morphology of the samples are calculated. While the coating rate decreases according to the iron concentration, fractal dimensions increase. However, as the number of clusters increases, the average cluster size decreases. The interface critical exponent value shows an irregular change.

1. Introduction

The way to switch to renewable energy sources and develop new energy vehicles is through energy storage technologies. Among them, rechargeable batteries and supercapacitors are two important energy storage devices. Compared to rechargeable batteries, supercapacitors are notable for their high power density and long cycle performance [1]. Among electrochemical supercapacitors, the energy storage of pseudo-capacitors (PCs) is based on rapid Faradaic and reversible reactions on the surface of the sample [2]. There are a lot of PCs studies with using different kind of materials such as bismuth enriched materials [3], transition metal oxides and chalgonides [4] and carbon nano-composites [5]. In recent days, various efforts have been made by different research groups to develop PCs based on transition metal oxides(TMOs) due to their high theoretical capacity (~600–1000 mAh/g) and several oxidation states to obtain necessary charge for redox reactions [6]. However, ongoing limited industrial using still is a huge problem due to low capacity and active sites of TMOs. Among TMOs, Co_3O_4 is so attractive with its superior theoretical specific capacitance (3560 F g^{-1}) and mixed valence with chemical stability. It is also often used in paramagnetic, solar cells, electrochromic devices and rechargeable batteries [7–9]. The nano- and microstructures of the Co_3O_4 electrodes prepared by different methods have electrochemical performance that varies according to each other. Soltani *et al* showed that the Co_3O_4 structures produced by spray pyrolysis with an average grain size of 30 nm which exhibited a specific capacity of 1800 F g^{-1} at a scan rate of 10 mV s^{-1} [10]. Chemical bath deposited Co_3O_4 electrodes showed specific capacitance of 1576 F g^{-1} as an electrode in another study [11]. With using cathodic electrodeposition, binder-less porous crosslinked nano flaky/flakes formed Co_3O_4

Table 1. Some Co_3O_4-based heterostructure studies in the literature.

Material	Application	Method	Reference
Fe_2O_3/Co_3O_4 heterojunction	Ethanol gas sensor	sol–gel auto combustion reaction	[17]
Fe_2O_3/Co_3O_4 heterojunction	Non-enzymatic dopamine sensor	sol–gel auto combustion reaction	[18]
ZnO/ Co_3O_4 heterojunction	Self-powered broadband photodetectors	spin coating	[19]
Co_3S_4 /Co_3O_4 heterojunction	CO gas sensor	two-phase hydrothermal and chemical vapour deposition (CVD)	[20]

electrodes exhibited a specific capacity 187.1 $mAhg^{-1}$ in 1 M KOH aqueous electrolyte at 5 mV/s scan rate [12]. Zn doping (between 2% and 10%) effect on the electrochemical properties was investigated by Asl *et al* and the highest value of areal capacitance was found to be 5.37 mF/cm2 for 6 at.% Fe: Co_3O_4 [13]. From these results, it has been seen that controlling the surface composition of the structures is still a challenging but has been mandatory for investigating active sites and reaction mechanism. Cobalt oxide films, which usually have three different type crystal forms such as s CoO, Co_2O_3, and Co_3O_4, are often preferred to improve their properties with doping atoms. This useful strategy, which causes changes in the host lattice and surface charge distribution of the cobalt oxide material, can often be achieved with metal atoms [14]. Iron is so proper as a metal doping atom due to similar ionic radius with cobalt and different 3d orbital electron numbers [15]. With using nebulizer spray pyrolysis, 1.366–1.713 eV and 2.846–2.925 eV for lower and higher energy regions for Fe: Co_3O_4 films and the maximum specific capacitance value is observed in the 2.5 wt% of Fe doping [16]. Finally, the following table 1 summarizes the characteristics of some Co_3O_4 -based heterojunctions;

Herein, pure and Fe:Co_3O_4 films have been rationally fabricated through a facile chemical bath deposition method. In this study, efforts were made to understand the effect of Fe doping on the structural, microstructural and electrochemical properties of Fe:Co_3O_4 thin films together with detailed surface fractal analysis. For the first time, the critical exponent values for the hetero-morphological structure produced in pure Co_3O_4 and different w % Fe concentrations were determined.

2. Methods

All chemicals were analytical grade, used without further purification and purchased from Sigma-Aldrich, ⩾ 99%. Before the thin film deposition, In: SnO2(ITO) the coated glass plates were soaked in boiling water with detergent, cleaned with alcohol, rinsed in distilled water and dried in an air environment to complete the substrate cleaning procedure. Pure Co_3O_4 and Fe: Co_3O_4 films were produced by chemical bath deposition. Briefly, 0.15 M $Co(C_2H_3O_2)2H_2O$, 3.26 g urea/KOH and $FeCl_3.6H_2O$ with different ratios of 2, 4 and 6 mol % were added to the bath containing 50 ml of distilled water. Precursors and complex agent separately were added. After magnetically stirring of aqueous solution, it was heated to ≈ 80 °C and ITO substrates were immersed in the resulting homogeneously distributed solution and left for 4 h. Following deposition, the pure Co_3O_4 and Fe: Co_3O_4 samples were dried at room temperature along one day and finally calcined at 400 °C for 1 h to remove residual material in air. The phase evolution and structural parameters of the produced samples were monitored by powder x-ray diffraction (XRD). x-ray patterns were recorded by Rigaku Smart-Lab x-ray diffractometer with using CuKα radiation between $2\theta = 5°$–$80°$ range. Scanning electron microscopy (SEM) was performed on a JEOL-7100F model microscope in connection with OXFORD Instruments X-Max energy dispersive atomic x-ray spectroscopy (EDAX). Atomic force microscopy (AFM) were conducted by Witec alpha 300 RA with non-contact mode ($5 \times 5\ \mu m^2$). Electrochemical experiments were realized standard three-electrode configuration [the active material and served as the working electrode, silver/silver chloride (Ag/AgCl) as a reference and a square Pt foil as the counter electrode] in 5 mM ferricyanide including 0.1 M KCl supporting solution as the electrolyte and scan rate was 50 mV s^{-1}. Impedance curves were performed using a Compactstat Interface (Ivium Technologies-Eindhoven,The Netherlands) and Autolab PGSTAT 128 N Potentiostat //Galvanostat equipped with a FRA2 frequency response analyzer under the frequency range of 10^{-1} to 10^5 Hz. All measurements were realized at room temperature.

3. Results and discussion

3.1. Structural properties

In figure 1, x-ray patterns of pure and Fe: films were shown in the $2\theta = 5°$–$80°$ range. Sharp peaks and polycrystallization were confirmed by x-ray patterns in each of samples. Well defined peaks correspond to cubic Co_3O_4 planes [(220), (311), (511), (440) respectively] were observed according to JCPDS: 00-009-0418 [15]. All samples had a major peak of (311) at ~37° which corresponding to preferential orentation of the films. In addition, substrate (ITO)- related peaks were detected especially un-doped Co_3O_4 samples due to low interaction between coated Co_3O_4 film and substrate. Cubic Co_2O_3 peaks were indexed

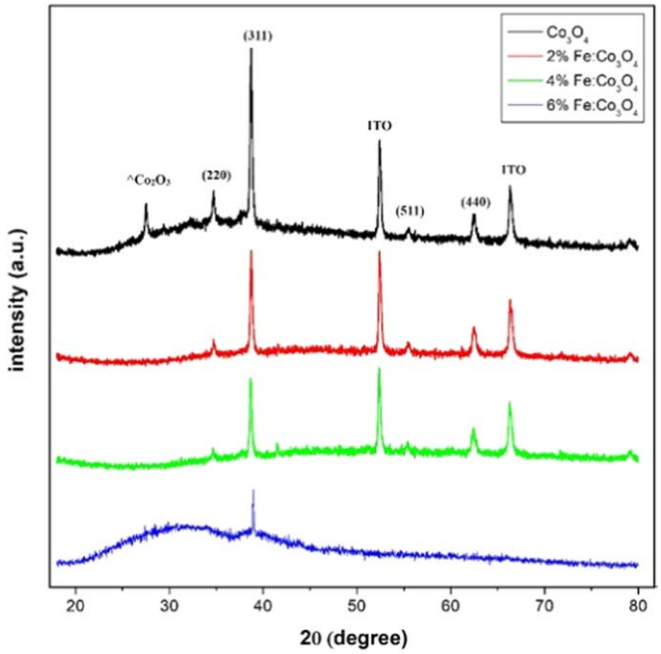

Figure 1. X-ray diffraction (XRD) patterns of (a) pure (black) and Fe: Co_3O_4 films [2% Fe(red), 4% Fe (green) and 6% Fe (blue)].

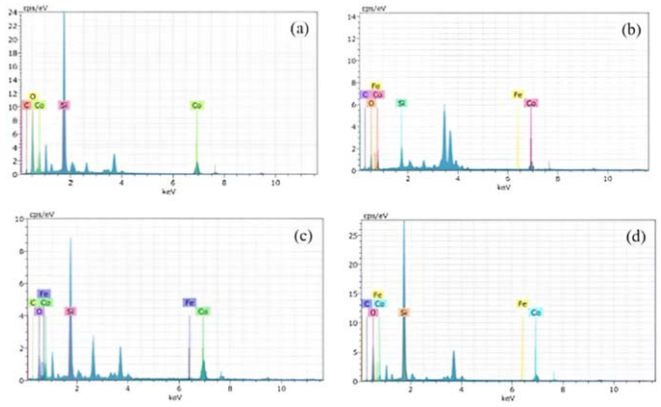

Figure 2. EDAX spectrum of (a) pure Co_3O_4, (b) 2% Fe: Co_3O_4, (c) 4% Fe: Co_3O_4 and (d) 6% Fe: Co_3O_4 samples.

in pure and 6%Fe- including samples with small intensity according to JCPDS: 76–1802 [16]. According to Debye–Scherrer formula, as shown at below (equation (1));

Figures 2(a)–(d) represents the EDAX spectra of deposited films at different iron concentrations (2, 4 and 6%). The carbon signal originates from the mesh holding the sample in EDX, while the silisium signal originates from the substrate [21].

$$D = \frac{0.94\lambda}{\beta \cos\theta} \quad (1)$$

where, D represents the average crystallite size, β presents the full width at half maximum (FWHM) of the peak, θ represents the Bragg angle, which corresponds to half of the diffraction angle. For preferential orientation of (311) plane, measured average grain size of the samples 48, 42, 44 and 56 nm for pure Co_3O_4, 2% Fe: Co_3O_4, 4% Fe: Co_3O_4 and 6% Fe: Co_3O_4, respectively. Substitution doping occurs when Fe ions are introduced into the Co_3O_4 host lattice, effectively substituting some Co ions [17]. However, formations in the form of agglomeration determined in the SEM images create problems in this scenario.

3.2. Morphological properties

Figure 3 displays surface images of pure and Fe-doped Co_3O_4 films were visualized using scanning electron microscopy (SEM) and particle sizes are between 30–200 nm range with heterogenous distribution. Agglomerative cluster forms were determined in pure, 2% and 6% Fe-doped Co_3O_4 samples while 4% Fe-doped Co_3O_4 sample exhibited porousstructures in the form of a network. Such porous structures provide

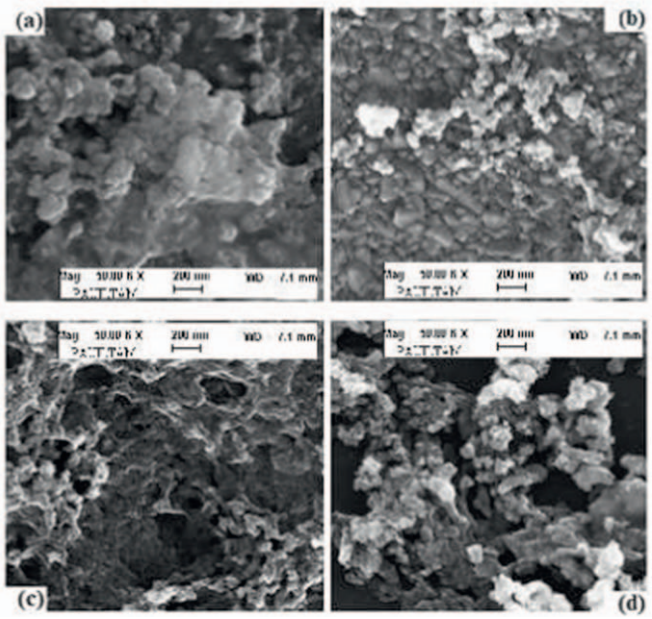

Figure 3. SEM images of (a) pure Co_3O_4, (b) 2% Fe: Co_3O_4, (c) 4% Fe: Co_3O_4 and (d) 6% Fe: Co_3O_4 surfaces.

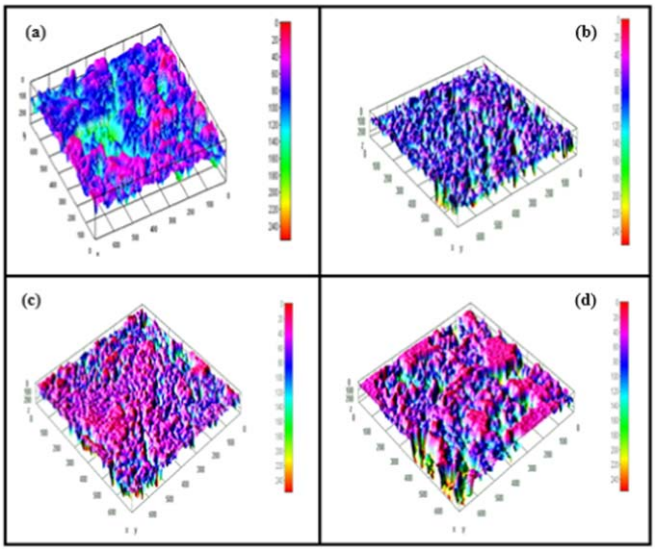

Figure 4. The 3D topographic images of (a) pure Co_3O_4, (b) 2% Fe: Co_3O_4, (c) 4% Fe: Co_3O_4 and (d) 6% Fe: Co_3O_4 specimens.

a large specific surface area for electrolyte access and reduce the diffusion path in the solid phase [22]. In addition, heterogeneous nucleation has an effect on the Co_3O_4 film growth that nucleation on the substrate surface in solid form reduces the surface energy. In this study, statistical scaling properties of surface heteromorphologies were determined using scaling method (fractal analysis) [23–25]. The dimensions of the samples are 51.20 nm × 38.40 nm (1024 pixels × 768 pixels, 8-bit magnification 5Kx) as standard. Micro-images of the samples were transferred to the computer and digitized. Images representing the optimum morphological structuring were selected from the square mesh with an edge size of L × L = 700 pixels × 700 pixels on the SEM image surfaces of thin films produced according to different concentrations. While figure 3(a) shows the surface image of the pure sample, the surface images of the specimens with 2%, 4% and 6% Fe concentrations are given in figures 3(b)–(d), respectively. Similarly, the three dimensional (3D) topographic image for the pure sample is given in figure 4(a), while the topographies of the samples with 2%, 4% and 6% iron concentrations are given in figures 4(b)–(d), respectively.

When the surface hetero morphology of the samples is examined, it is seen that structuring of specimens are microscopically amorphous. In the surface formations of the materials, a structuring similar to island, mountain, valley and cave formations has been determined, and it has been observed that there are

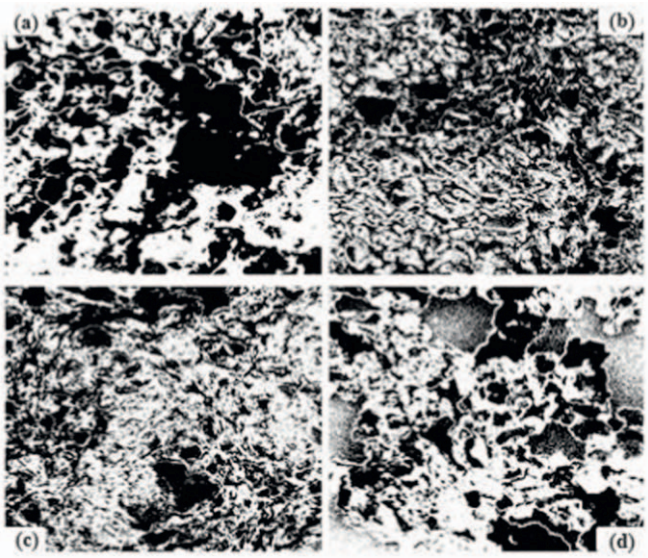

Figure 5. The BMP images for (a) pure Co_3O_4, (b) 2% Fe: Co_3O_4, (c) 4% Fe: Co_3O_4 and (d) 6% Fe: Co_3O_4 samples.

partial voids in some regions. In addition, it was predicted that the regional brightness difference of the patterns in the film surface images and the changes in hetero morphology may be caused by the iron concentration in the electrolysis liquid during production. Figure 5 exhibits digitized SEM images of samples in bitmap (BMP) format. Holistic structures are observed in figures 5(a)–(c) for the pure, 2% and 4% compositions, but a thin layered structure is observed on the glass in figure 5(d) for sample containing 6% Fe composition. When the nano-heteromorphic structure is examined, it consists of fractal and non-fractal cluster patterns that are dependent or independent, varying in size and position. In such cases, each cluster pattern can be defined as the sum of the cellular particles of the mesh surface grid.

The scaling method is an important method to identify the self-similar configuration of observable amorphous and superficial hetero-morphous sample surfaces. In general, scaling applications can be defined by a simple exponent-law relationship independent of the formation conditions of the system. This method is generally preferred for statistical physics approaches to the system and photometric applications. SEM images of the samples are transferred to the personal computer atmosphere using ImageJ and digitized with software [25]. However, before starting the scaling calculations, it is accepted that for the applicability of the methods, density verifications in the images of these surfaces, rather than the morphological structure on the surfaces themselves. Gaussian blur is filtered with A = 2 value to increase the saliency of morphological change in sample images. In the first step, images are converted to bitmap (BMP) format to define the morphological formation of the sample surface and identify particles. Afterwards, calculations of scaling operations and morphological dimensionality evaluations are applied [26].

The morphological structure of the sample surfaces has a cellular image density and each is defined as a particle. The sums of independent particles on the sample are determined as Si representing cluster patterns. The visible patterning of the particles on the sample surface has two different superficial coverage ratios. One of them is the cellular particle occupancy in the image carried to the mesh surface. The heteromorphic thin film sample image is digitized in bitmap format and cellular particle densities are determined as shown in figures 6(a)–(d). According to the scaling theory [25], the particle density of the cell with position xi, yj on the mesh surface is proportional to the cell size value $\in = 1$ pixel in BMP format. The particle density is defined as:

$$\rho(x_i,\ y_j) = \begin{cases} 1, & \text{if site is black,} \\ 0, & \text{else white.} \end{cases} \tag{2}$$

The second term is the surface particle coverage ratio A, which gives the probability of being in any xi, yj location and is defined as the ratio of the total number of particles to the lattice surface in the surface configuration. The particle coverage ratio is expressed as:

$$\phi\ (N,\ L) = N(\rho\ )L^{-d} \tag{3}$$

where $N\ (\rho) = \sum \rho(xi,\ yj)$ nLx, Ly i, j is the total number of particles and d = 2 is the Euclidean dimension value. In the pure and Fe-doped specimens, the surface image intensity is considered between 1 and 255, and the variation of the surface image density according to the lattice edge is determined. The surface histogram of the materials and the cellular image densities are given in figures 6 and 7.

The other morphological parameter, fractal dimension, is a useful quantification for characterizing scholastic composite growth and its relationship to both

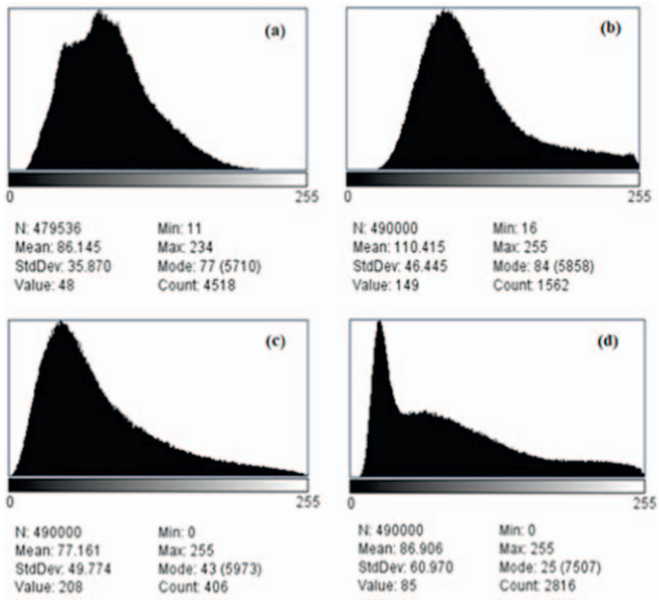

Figure 6. The surface histogram plots of (a) pure Co_3O_4, (b) 2% Fe: Co_3O_4, (c) 4% Fe: Co_3O_4 and (d) 6% Fe: Co_3O_4 samples.

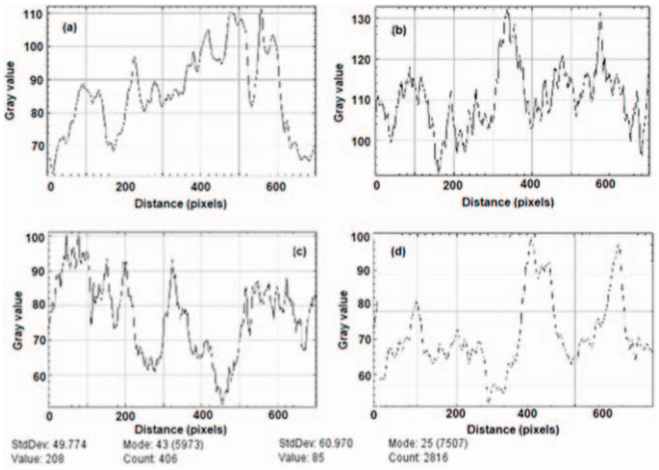

Figure 7. Surface image density (intensity) change in hetero morphological structure of (a) pure Co_3O_4, (b) 2% Fe: Co_3O_4, (c) 4% Fe: Co_3O_4 and (d) 6% Fe: Co_3O_4 samples.

morphological pattern and tissue properties. The fractal dimension df is usually calculated using the scaling method to quantitatively describe heteromorphic structures and determine cluster structure on the surface [23–25]. The fractal dimension is a measure of the complexity of the surface structure in metals [24, 25]. The variation in the detail in the structuring can be explained by the change of the reference scale in determining the structuring features. Therefore, as a result of the electrodeposition of iron concentration, information can be obtained about the scalability of the morphological structure, particle distribution and cluster formation. In general, fractal size, particle density, and the number of groups belonging to the same particle size are proportional to the (∈) scale used for N (∈). The relationship between scale (∈) and the number of particle density groups N (∈) can be expressed as:

$$N(\in) \sim \in^{-d_f} \quad (4)$$

Fractal dimension value analysis for heteromorphic structure can help to quantitatively categorize island- structured cluster patterns on the sample surface. The fractal dimension df is a parameter that represents the complexity of self-similar fractal pattern forms. It is convenient to calculate the fractal dimension to characterize the structure of cluster patterns on the surface. and the pattern structure formed by the particle distribution. Many different methods and algorithms are used to calculate the fractal dimension. In this study, the box-counting method [26] was used. Obs N(∈) ∼ ∈ −dfervable formation forms for the first layer of the sample surface are moved into the square mesh with various edge lengths and filled pixels (∈) are determined. The number of pixels filled as particles is scaled as N (∈) as indicated in the following

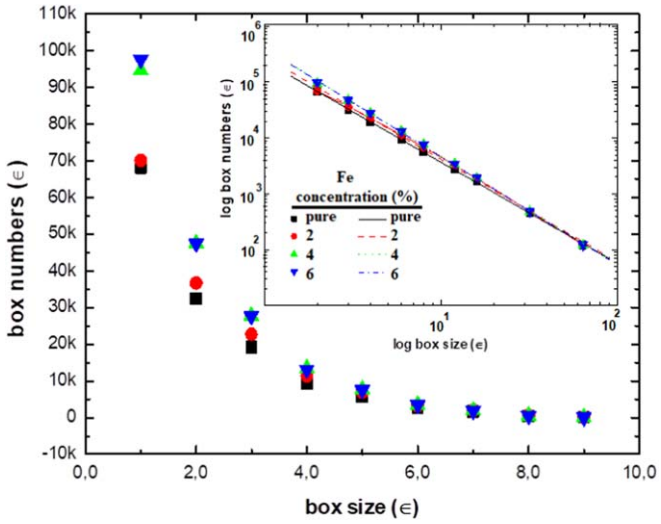

Figure 8. The variation of the particle density size ∈ value depending on the particle group number N(∈).

equation. Usually, a data distribution is created regarding the number of particles in the image. The fractal dimension is extracted from equation (5);

$$d_f = \frac{-\log N(\in)}{\log(\in)} \quad (5)$$

where N(∈) represents the number of pixels that make up the morphological configuration or the number of frames according to the computer screen scale, and ∈ represents the size of the smallest filled cells of the pixel particles that make up the variation in the configuration. The numerical calculation of the fractal dimension involves a step-by-step iteration algorithm. After each processing step, the cell size ∈ value is increased and the number of particle groups formed N(∈) is determined. In the box-counting algorithm used in this study, two (∈ = 2i pixels i = 0, 1, 2, 3, 4…) values are also calculated and the log N(∈) versus log ∈ data distribution is plotted. In general, distributions relations for morphological construction datasets are linear, and the absolute value of the slope calculated by linear regression method correspond to the fractal dimension df [27]. Figure 8 shows the data scatter plot of the particle density size ∈ value depending on the particle group number N(∈). In addition, fractal dimensions are calculated from the slope values of the linear regression trend graph log ∈ - log N(∈). For the observable structure of each sample, the surface particle coverage ratios and fractal dimensions are 49.36% and 1.805 for the pure sample, 40.45% and 1.832 for the 2% Fe-doped sample, 37.561% and 1.930 for the 4% Fe-doped sample, and 31.00% and 1.933 for the 6% Fe-doped sample. The regression coefficient for linear regression calculations was determined as ($r2 > 0.999$), which indicates that scaling and fractal analysis methods can be applied for the characterization of the thin film surface. In addition, the variation of the coating ratio of the thin film produced by adding different concentrations of Fe into Co_3O_4, depending on the fractal dimension, is shown in figure 8.

The fractal dimension increases while the surface coverage ratio decreases with respect to the Fe concentration. This is an expected result, as the increase in Fe concentration in the system will decrease the mobility of Fe ions in the liquid, provided that the production conditions remain the same. When the system created for production starts to work effectively, Fe ions are reduced and added to the core particle cluster on the surface and form the multi-layered layer. The aggregation of Fe ions on the surface of the Co_3O_4 liquid implies the particle aggregation with fractal size of ~1.72 and the DLA model formed by the particles exhibiting Brownian motion behavior in the literature [26, 28, 29]. In similar studies in the literature, fractal size values of natural manganese deposits on the magnesite ore surface vary between 1.626 and 1.740 [29]. These formations are very dense and vary according to the surface location. In one of the pioneering studies of Matsushitai *et al*, the fractal dimension value of the tree-like dendrite structure on the zinc (Zn) linear electrode was reported as 0.70 ± 0.06 [30]. Haniam *et al* observed fractal structures on the thin film surface produced by cobalt oxide (CoO and Co_3O_4) at room temperature and pressure laser deposition method and reported that the fractal dimensions vary between 1.499 and 1.759 [26]. Due to the growth of chromium (Cr) thin film on the silicon substrate, aluminium (Al) and then cobalt (Co) thin film on it, these values show that the cluster pattern structure on the active sample surface is dendrite structure. In addition, in this study, they suggested that the sample surface aggregations can be described with the DLA model [26]. However, although the fractal dimension value in the pure Co_3O_4 thin film produced in this study is compatible with this study, the fractal dimension increases in the surface structure formed as a result of adding Fe at different concentrations to the production. This shows that the addition of Fe increases the density of the clusters in the surface structure.

Table 2. The estimated fractal analysis parameters in comparison with the literature.

Co_3O_4 thin films	Fe concent. (%)	Coverage rate (~% σ)	Fractal dimension (d_f)	Regression constant R^2	Cluster number (n_c)	Main cluster (s nm^2)	Main cluster (s nm^2)	Interface exponents* $^{(\tau)}$
(a)	Pure	49.36	1.811 ± 0.010	0.9998	290	33.50	27.531 ± 3202.321	1.313 ± 0.139
(b)	2	40.45	1.838 ± 0.030	0.9981	2060	17.35	20.680 ± 0.159	1.677 ± 0.186
(c)	4	37.56	1.934 ±	0.9992	1758	16.45	27.641±	1.213±
(d)	6	31.00	1.938±	0.9995	2059	12.56	28.055±	1.783±
Cobalt oxides (CoO ve Co_3O_4) [29]			1.49 9–1.759	—	—	—	—	
DLA simulations [28]			1.720	—	—	—	—	1.55
Zinc (Zn) clusters [28]			0.70 ± 0.06	—	—	—	—	1.54
Natural manganese deposites [29]			—	—	—	—	—	1.054–1.321

* Present study

The surface particle coverage rates, fractal dimensions and the number of observable clusters calculated as a result of examining the cluster structures of the sample surface are summarized and presented in table 2. The number of particles was determined as 622 for the pure sample with a surface coverage rate of 49.36%, 2865 for the sample with 2% concentration with a coverage rate of 45.40%, 2887 for the sample with 4% concentration, and 1963 for the sample with 6% concentration. It was revealed that the number of independent clusters increased when the Fe concentration increased. This situation can be considered as an indication that when production starts, Fe ions are reduced due to electrical effects and initiate the nucleation effect on the surface. It can be said that the combination of other reduced ions with the cluster increases the growth at different rates. This result shows that the thin film surface has anisotropic properties. It is expected that the electrical conductivity of the sample will be positively affected as a result of the increase of the possibility of contact of the conductive particles on the surface of the material as a result of the growth of the clusters and the formation of a conductive network in the material. There is a relative uncertainty of measurement in the calculation of the fractal dimension. Accordingly, the measurement uncertainty can be defined by the relation Δdf df and the standard deviation by the relation $\Delta df = df - df$.

The measurement uncertainty in fractal dimension was calculated as 2.5% for the pure sample, 3.1% for the sample with 2% Fe concentration, 1.5% for the 4% Fe concentration, and 6% for the Fe concentration. The electrolyte liquid concentration used in thin film production can have an effect on the clump or particle size of the resulting film. In general, increasing the concentration of the electrolyte solution can lead to a reduction in the size of the clumps or particles formed during deposition. This is because when the concentration of the electrolyte solution is high, the ions are packed more closely together. Thus, when ions accumulate on the electrode (substrate), they are more likely to collide with each other and form smaller clumps or particles. In this study, cluster formation and cluster size behaviour that can be observed in heteromorphic structuring of Co_3O_4 thin film surface produced by adding pure and different concentrations of Fe were investigated. It should be noted, however, that the relationship between electrolyte concentration and cluster or particle size is not always simple and negligible. There are many other factors that can also affect the size and morphology of the clumps or particles, such as the deposition rate, the temperature and pressure of the deposition medium, the type of electrode, and the chemical properties of the electrolyte solution itself. In the sample surface configuration, any cluster pattern size si is nk times the number of particle densities. Thus, any cluster size is proportional to the total number of accumulated (cumulative) particle density, with the cellular quantitative mass value of each particle. In addition, the mesh dimensions are determined in L × L∈ (xi ve yj) cell coordinates where it means the sum of the cumulative number of cluster particles. Cluster pattern size is expressed by the following relation:

$$s_i = \sum_{i,j=1}^{n_{i,j}} n_k \, \rho(x_i, y_j) \tag{6}$$

The size and number of observable cluster patterns are proportional to the cellular image density and scale value formed according to the pure and Fe concentration of the sample image. Cluster size was determined at a scale of 0.1675 pixels/μm. The total number of observable clusters on the sample surface is nc, the number of observable clusters for the pure sample is 290 with different positions and their size varies in the range of $1 \leqslant si \leqslant 1413$ nm^2. When 2% Fe is added to the sample, 2060 clusters with sizes ranging from $1 \leqslant si \leqslant 4845$ nm^2, 1758 clusters with 4% doping, and, 2059 clusters with sizes ranging from $1 \leqslant si \leqslant 2729$ nm^2 at 6% concentration were determined. When the hetero-morphology of the undoped, 2% and 4% doped samples is examined, it is determined that the particle aggregation is in the form of aggregation and is made in the form of heaps in the direction perpendicular to the surface, while the pore structure is dominantly observed on the surface of the 4% Fe doped sample. The fractal dimensions for the samples vary

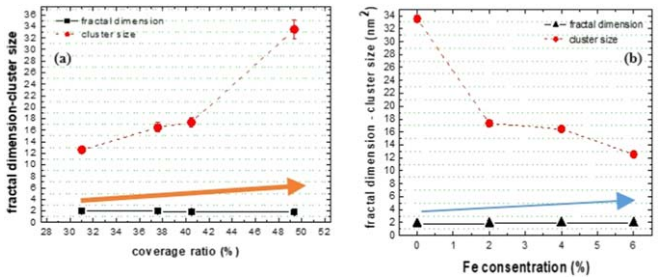

Figure 9. (a) The variation of fractal size and cluster size with surface coverage ratio, (b) the variation of fractal size and cluster size with Fe concentration.

between $1 \leqslant d_f \leqslant 2$, but the cluster size varies between ~~12 nm^2 $\leqslant s_i \leqslant$ ~ 34 nm^2 figure 9 shows the change in fractal dimensions and cluster sizes depending on the coating rate and Fe concentration. Since the fractal dimensions are quite small compared to the change in cluster size, the change in fractal dimension is shown with red and blue arrows. Additionally, fractal dimensions and cluster size values are presented in table 2.

As can be seen from and figure 9(a), fractal dimensions and cluster size increase with coverage ratio. However, it is seen that the cluster size decreases with increasing Fe concentration as shown in figure 9(b). Since the increase in the number of clusters when doped with Fe will increase the effective current density in different systems, it is predicted that it may have a positive contribution to the conductivity. It is an expected result that while the number of clusters increases in the structuring of the Fe doped thin film surface, the cumulative accumulation size values of the cluster patterns decrease. Because, during the electrodeposition process of pure Co_3O_4 ionic liquid, firstly Co_3O_4 precipitates and aggregation begins when it sticks on the surface with the effect of adhesion forces. It accumulates on the surface and shows distribution according to the effective value of the electrical equipotential values on the surface. As a result of adding different concentrations of Fe to the Co_3O_4 liquid used in the other production step, Co_3O_4 is first reduced and a solid phase begins to form on the electrode surface. In the meantime, Fe particles accumulate at the interface between the cluster surface and clusters and make a significant contribution to aggregation. At the same time, this can also change the magnetic properties of the thin film. Therefore, adding different concentrations of Fe can enable the sample to switch to a new magnetic and morphological phase state, and it can be expected that the critical distance value between clusters will increase the effect on the electrical properties. The cluster pattern density parameter is defined as the ratio of the number of independent clusters to the lattice surface and is an important parameter for Fe-doped Co_3O_4 thin film surfaces at different concentrations. The cluster pattern density can be defined as:

$$\bar{n} = L^{-d} \sum_{i,j=1}^{n_{max}} n(s_i) \tag{7}$$

Cluster density was calculated as 4204.10^{-6} for pure material, 3588.10^{-6} for 2% Fe added, 592.10^{-6} for 4% and 2847.10^{-6} for 6%, respectively. As the coverage rate decreases for the samples, the cumulative cluster mass decreases and the number of observable clusters on the Fe- doped sample surfa

ces increases. Therefore, it has been revealed that when the Fe concentration increases, the possible roughness will decrease as a result of the decrease in the cluster size and its distribution on the surface. This implies that there are more interacting surface locations on a different contact surface. In addition, it was reported that the distance between clusters decreased and this result was found to be compatible with the literature [23–27]. This situation contributes positively to the electrical conductivity, electrical behaviour and polarization of the clusters during electric current. The scaling behaviour approach for samples is proportional to the cluster size and the number of clusters. The relationship between the number of cluster patterns on the Fe- doped Co_3O_4 thin film surfaces at different concentrations and the cluster pattern size si $\geqslant$ 1 nm^2 in the limited-size square mesh shows the scaling behaviour and can be described by the following equation.

$$n(s_i) \sim s_i^{-\tau} \tag{8}$$

where τ is the critical exponent defined for the interfaces according to the scaling theory [24]. This relationship can be used for cluster pattern sizes with respect to Fe concentration, and cluster size values are said to show scaling behaviour between the values at which repetition ends. For undoped Co_3O_4 thin film surface structuring $1 \leqslant si \leqslant 1413\,\mu m^2$, for 2% Fe concentration doped $1 \leqslant si \leqslant 5671\,\mu m^2$, for 4% Fe concentration doped $1 \leqslant si \leqslant 4845\,\mu m^2$, for 6% Fe concentration added $1 \leqslant si \leqslant 17704\,\mu m^2$. The critical exponent values of each sample were calculated between $\approx 10\,\mu m^2$ and $\approx 500\,\mu m^2$, ignoring the extremely small or excessively large values that distorted the statistical distribution and using the linear regression method. Accordingly, the critical exponent values were calculated as 1.313 for pure Co_3O_4, 1.677 for the sample with 2% concentration, 1.213 for the sample

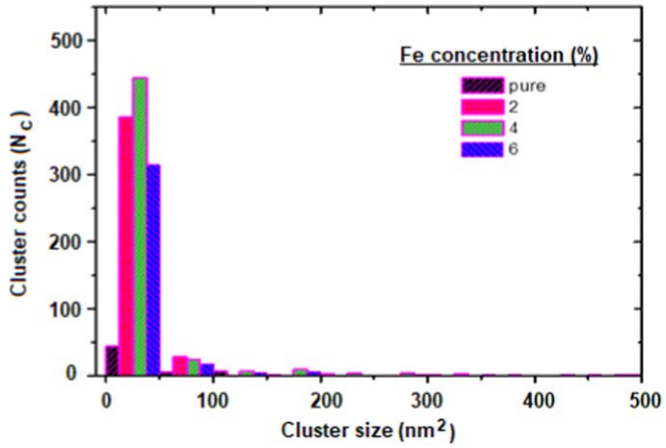

Figure 10. Histogram of the relation of cluster size with the number of clusters.

with 4% Fe concentration and 1.783 for the sample with 6% Fe concentration, respectively. The regression coefficient in linear regression calculations was calculated as r2 > 0.92785. According to the results obtained from the samples, the interface critical exponent shows an irregular change. This result implies that the structuring surface of the clusters is quite large and the distances between the clusters are small. These results show that the superficial tissue restructuring is regular and effective. It has been determined that the resulting cluster representations are dendrite structuring. In the literature, studies on critical exponent values for a single delimited cluster with hetero-morphological structure have been carried out. Meakin determined the interface critical exponent value as $\tau = 1.55$ for the cluster representations produced by the DLA Model algorithm using the Monte Carlo technique in the two-dimensional square lattice [31]. In another study, Matsushita *et al* reported the critical exponent value of 1.54 for the three-dendrite-like patterns of zinc (Zn) metal obtained by electrodeposition [30]. The critical exponent value for natural magnesite surface dendrite manganese dendrite cluster groups was determined as 1.054 to 1.321. However, in this study, for the first time, the critical exponent values for the hetero-morphological structure produced in pure Co_3O_4 and different Fe concentrations were determined. As in the 4% Fe doped sample, the uneven cluster growth during fabrication causes a change in the scaling behaviour as a result of the finite size effect. In this sample, the porous structure on the surface plays an active role rather than the cluster structure.

The number of clusters on the sample surface is closely related to the repetition of clusters of the same size. In this study, the change in the sample thin film surface structure, with the cluster size si $\in$ R + and the number of valuable clusters N (si), is shown with the histogram graph in figure 9. In addition, the cluster mean was also calculated by the classical method and the results were recorded in table 2. A Gaussian distribution function can be defined statistically for clusters. In this definition, the cluster size and the distribution function of the number of observable clusters of the same size are expressed as:

$$N(s_i, w) = \frac{A}{w\sqrt{\pi/2}} \exp\left(-2(s - \bar{s})/w\right)^2 \qquad (9)$$

where A is a fixed value, statistical median with $w > 0$ and $\bar{s}$ is the standard derivation, that is, the expected value. For the samples, firstly, repeated N (si) values were calculated according to the cluster size si values. Then, the smallest and largest values that distort the statistical distribution excessively are neglected. The average cluster size was calculated statistically by applying the nonlinear regression method to the system. The mean cluster size values were calculated as 27.531 μm^2 in the pure sample, 20.641 μm^2 in the sample with 2% concentration, 27.641 μm^2 in the sample with 4% Fe concentration, and 28.055 μm^2 in the sample with 6% Fe concentration, and it was determined that it showed an irregular variation. Figure 10(a) shows the log Nc(si) versus log si while figure 10(b) shows variation of cluster size with the number of clusters in the column chart. The results were calculated by both the classical method and the statistical method and recorded in table 2. It can be seen from the results that for classical mean calculations, the sample surface cluster size tends to decrease with increasing concentration. It would not be correct to generalize this result, since in classical calculation, only one image from each production condition is studied instead of a crowded sample set. In addition, as seen in figure 11, in the statistical calculation, the mean cluster size behaved in direct proportion to the concentration.

The formation of independent clusters of pure and different Fe concentration-doped Co_3O_4 film surface, especially at pure, 2% and 6% values, resembles partially Eden and DLA model simulation representative clusters. While Co^{+4} is reduced on the electrode, O^{-2} gas exits the system with the effect of the current created as a result of the electrical potential applied during production, and accumulates on the different $Fe^{+2,+3}$ concentrations and Co^{+4} electrodes by being

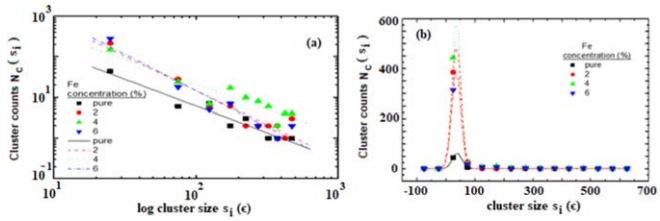

Figure 11. (a) Variation of logarithms of cluster number and cluster size (b) Variation of the number of clusters calculated with the least squares method with the cluster size.

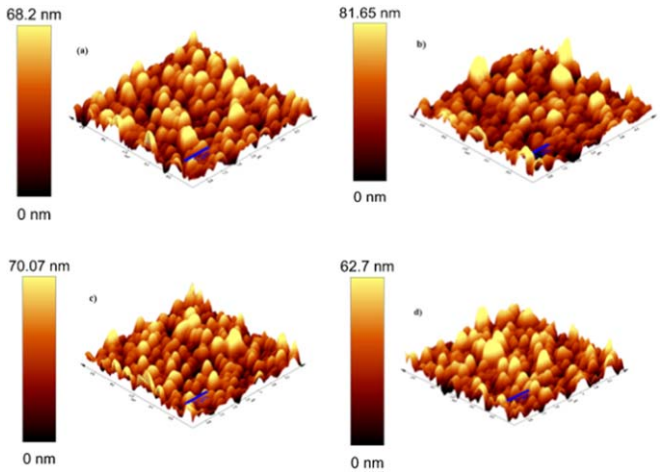

Figure 12. 3D AFM topography images of (a) pure Co_3O_4, (b) 2% Fe: Co_3O_4, (c) 4% Fe: Co_3O_4 and (d) 6% Fe: Co_3O_4 surfaces.

Table 3. Roughness values of pure Co_3O_4 and Fe: Co_3O_4 film surfaces.

Sample	Average roughness (S_a) (nm)	Root mean square roughness (S_q) (nm)
Pure Co_3O_4	34.24	44.14
2% Fe: Co_3O_4	76.78	90.41
4% Fe: Co_3O_4	24.01	29.76
6% Fe: Co_3O_4	22.91	28.51

reduced. The electrical potential gradient (electric field) increases the mobility of the ions, and the electric field that occurs in parallel with this situation ensures that the ions are reduced and accumulated on the electrode. Therefore, the increase in mobility also increases the mean free path of the ion particles, and thus, the particle aggregation occurs by increasing the interaction area of the particles on the electrode. If the concentration of reduced reactance in the system is increased, more reactance particles are formed that move together. Therefore, more collisions occur between Fe ions and therefore the effective reaction rate on the electrode increases. As the concentration of the reactants increases, the reaction rate also increases. With the increase of the concentration, the size of the cluster formed by the fluctuation of the concentration value on the electrode surface decreases and the surface area forming the cluster increases. The smaller particle size of the reactants provides a larger surface area where collisions can occur. The increase in the surface area value increases the reaction rate proportionally. Reducing the size of the particles, smoother surface quality, increased conductivity, increased number of clusters and reduced coating during construction, higher particle packing properties are the properties sought in high quality materials.

To determine the variation of thickness, three-dimensional (3D) AFM topography of selected film areas are shown for scanning area ($5 \times 5\,\mu m^2$) in figure 12. The rough change on the film surface with lump and agglomerated particles is obvious in 2% Fe: Co_3O_4 samples. Pointed island formations scattered heterogeneously on the surface for all samples while a decrease in the size of these formations are observed in 4% Fe:Co_3O_4 samples. In table 3, roughness values for the deposited films were presented. With increased Fe doping, the roughness on the film surfaces decreased, especially in 4% and 6% doped samples, which is possible due to the change in the crystallite size given in the figure 1(b). as a result of iron fusion in host cobalt oxide lattice [22]. It is known that it causes a significant change in electrochemical properties [32].

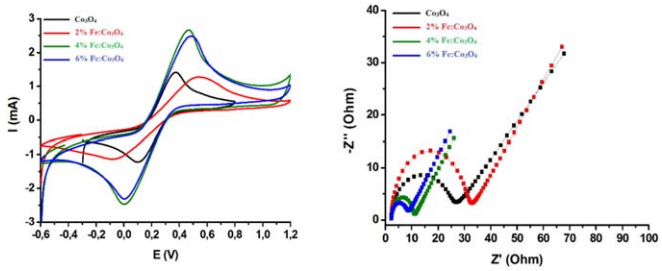

Figure 13. (a) Cyclic voltammogram (CV) were recorded in between −0.30 V- +0.80 V and −0.6 V - +1.2 V scan range and 50 mV s^{-1} was scan rate, (b) Nyquist plots and the equivalent circuit (insert) were obtained in the $10^{-1} - 10^{5}$ Hz frequency range of pure and Fe: Co_3O_4 electrodes.

Table 4. Circuit parameters for the pure and Fe: Co_3O_4 electrodes.

Electrode	E_a (V)	E_c (V)	I_a (mA)	I_c (mA)	R_{ct} (ohm)
Pure Co_3O_4	0,37	0,11	1,1	1,35	25
2% Fe: Co_3O_4	0,52	−0,05	1,17	0,89	31
4% Fe: Co_3O_4	0,46	0,13	2,4	2,1	9.2
6% Fe: Co_3O_4	0,48	0,01	2,2	2,1	7

3.3. Electrochemical properties

To understand kinetics of electrodes during charge/ discharge process, cyclic voltammetry (CV) measurements were realized. The representative CV curve of the pure and Fe: Co_3O_4 electrodes at a scan rate of 50 mV s^{-1} in the potential range of (−0.6–1.2 V) including 0.1 M KCl aqueous supporting electrolyte is demonstrated in figure 13. CV curves of the pure and Fe: Co_3O_4 electrodes, which exhibit well-defined redox peaks rather than rectangular shapes of the electrical double-layer capacitance, show that the resulting capacitance is mainly due to the Faradic pseudo-capacitance. Detailed charge–discharge mechanism was explained between electrode and ferricyanide by Dhakal *et al* [33]. Compared to pure Co_3O_4, Fe: Co_3O_4 has an ability to store more electrical charge during electrochemical reactions [28]. The area integrated into the CV curves was expanded at the Co_3O_4 electrodes with 4% and 6% Fe doped, which implies higher charge storage with increasing the active sites. It indicates the electrochemical performance of electrode material may vary depending on the morphology of the microstructure, as seen in similar studies [34]. The anodic peaks shift slightly from 0.37 to 0.46 V, working as long buffer reservoirs through the pore structure in the 4% iron-doped electrode, minimizing the effect of current polarization on electrode performance, as explained by Li *et al* [35]. The asymmetry seen in CV curves is due to the kinetic irreversibility in the cobalt oxide redox reactions [36]. As seen in table 4, although anodic potentials of 4% and 6% Fe: Co_3O_4 are similar, the increase in cathodic potential can be attributed to the porous structure of 4% Fe: Co_3O_4. The following equations are used to analyze the kinetic process of electrode materials in electrochemical reaction in more detail [37].

$$i = a\upsilon^{b} \tag{10}$$

$$\log i = b\log\upsilon + a \tag{11}$$

where the υ (mV s^{-1}) is scanning rate and i is the current of oxidation/ reduction peaks. The b value is corresponding to charge storage dynamic. The values of b for oxidation and reduction peaks were calculated as $0.5 < b < 1$, indicating the coexistence of pseudocapacitance in the electrode material. Electrochemical impedance spectroscopy (EIS) is described as a transfer function technique applied to electrochemical systems to evaluate the conductivity and ion transport kinetics [38]. It is used by analysis of impedance data and reduction of ferricyanide in a KCl supporting electrolyte to show the sensitivity of impedance to the development of electrode properties within frequency range of 10^{-1}–10^{5} Hz. As seen in figure 13(b), the Nyquist graph (plot of the imaginary component (Z″) of the impedance against the real component (Z′)) consists of a small semicircle in higher frequency regions and a straight line giving the Warburg impedance (Rw) in the low frequency regions, as well as two parts that can be attributed to the charge transfer process and ion diffusion in the electrolyte, respectively. The lower slope of the straight line in the low frequency range compared to pure Co_3O_4 electrode implies a larger Rw value related to the ion diffusion within the Fe: Co_3O_4 electrodes [39]. The charge transfer resistance (R_{ct}) of the 4% and 6% Fe-doped Co_3O_4 electrodes (the diameter of the semicircle at high-medium frequency) is significantly lower than that of the un-doped Co_3O_4 electrode, implying that ions have faster reaction kinetics along insertion and extraction in 4% and 6% Fe-doped Co_3O_4 samples [40]. These results show that the

charge transfer resistance (R_{ct}) is strongly affected by iron doping.

4. Conclusion

In summary, Co_3O_4 films succesfully deposited on the surface of ITO slides at various concentrations of iron (2, 4 and 6 mol %) by using facile chemical bath deposition. X-ray patterns demonstrated that a mixed Co_3O_4-ITO with/without Co_2O_3 structure was formed in all samples. Heterogeneous surfaces was observed from SEM and AFM images. When different concentrations of Fe were added to the pure Co_3O_4 sample, it was observed that the coverage ratio decreased, the fractal dimensions increased and the observable cluster surface area increased. While the cluster size decreased according to the Fe concentration, the number of clusters increased. It was observed that the thin film surface structure with 4% Fe concentration from the samples was porous and precipitated rather than agglomerated. It has been revealed that the addition of Fe at different concentrations to the undoped thin film provides a more regular structuring of the cluster distribution on the surface. The CV curve area and obtained plots from EIS show that 4% and 6% Fe:Co_3O_4 electrodes are suitable for electrochemical applications with its much more electro-active region compared to counterpart electrodes.

Data availability statement

All data that support the findings of this study are included within the article (and any supplementary files).

ORCID iDs

Fatma Sarf https://orcid.org/0000-0002-4445-4800
Aykut Ilgaz https://orcid.org/0000-0002-9632-0281

References

[1] Olabi A G, Abbas Q, Al Makky A and Abdelkareem M A 2022 *Energy* **248** 123617
[2] Jiang Y and Liu J 2019 *Energy Environ. Mater.* **2** 30–7
[3] Vadivel S, Hariganesh S, Paul B, Balasubramanian N and Rajendran S 2022 *Encyclopedia of Energy Storage* **1** 581–9
[4] Zhu X 2022 *Journal of Energy Storage* **49** 104148
[5] Potphode D and Sharma C S 2020 *Journal of Energy Storage* **27** 101114
[6] Fang S, Bresser D and Passerini S 2020 *Adv. Energy Mater.* **10** 1902485
[7] Bashir *et al* 2018 *Nanoscale* **10** 2341–50
[8] Yue X, Wang G, Wang J, Fan L, Hao J, Wang S, Yang M and Liu Y 2022 *Coatings* **12** 1682
[9] Vijitha S K J, Mohanraj K and Jebin R P 2023 *Chemical Physics Impact* **6** 100183
[10] Soltani S, Mohammad Rozati S and Mohammad Askari B 2022 *Physica B* **625** 413464
[11] Srinivasan V and Weidner J W 2002 *J. Power Sources* **108** 15–20
[12] Jadhav S L, Jadhav A L and Kadam A V 2022 *Electrochim. Acta* **426** 140845
[13] Asl H Z and Mohammad Rozati S 2023 *Chem. Phys. Lett.* **815** 140364
[14] Zhang W, Anguita P, Díez-Ramírez J, Descorme C, Valverde J L and Giroir-Fendler 2020 *Catalysts* **10** 865
[15] Guragain D, Karna S, Choi J, Bhattarai R, Poudel T P, Gupta R K, Shen X and Mishra S 2021 *Processes* **9** 2176
[16] Manickam M, Ponnuswamy V, Chinnasamy S, Ravindran S, Ramasamy M, Bose A and Chandrasekaran J 2017 *J. Mater. Sci., Mater. Electron.* **28** 18951–65
[17] Khan M *et al* 2023 *J. Mater. Sci., Mater. Electron.* **34** 1982
[18] Khan M, Abid K, Ferlazzo A, Bressi V, Espro C, Hussain M, Foti A, Gucciardi P G and Neri G A 2023 *Chemosensors* **11** 379
[19] Wang H, Zhou L, Li L, Gu Y, Kim B and Huang J 2024 *Opt. Mater.* **148** 114778
[20] Mingcong T *et al* 2024 *Sensors Actuators* B **401** 134968
[21] Abdallah A M and Awad R 2023 *J. Supercond. Nov. Magn.* **33** 1395–404
[22] Kucukarslan A *et al* 2021 *Appl. Phys.* A **127** 512
[23] Vicsek T 1992 *Fractal Growth Phenomena.* (World Scientific)
[24] Mandelbrot B B 1985 *Phys. Scr.* **32** 257
[25] Mandelbrot B, Passoja D and Paullay A 1984 *Nature* **308** 721–2
[26] Haniam P, Kunsombat C, Chiangga S and Songsasen A 2014 *The Scientific World Journal* **28** 685270
[27] Schneider C A, Rasband W S and Eliceiri K W 2012 *Nat. Meth.* **9** 671–5
[28] Witten T A and Sander L M 1983 *Phys. Rev.* B **27** 5686
[29] Bayirli M and Ozbey T 2013 *Z. Naturforsch.* A **68** 405–11
[30] Matsushitai M, Hayakawa Y and Sawada Y 1985 *Phys. Rev.* A **32** 3814–6
[31] Meakin P 1983 *Phys. Rev.* A **44** 2616
[32] Velmurugan R *et al* 2022 *Electrochim. Acta* **419** 140371
[33] Dhakal *et al* 2021 *Energy* **218** 119436
[34] Pietsch P, Westhoff D, Feinauer J, Eller J, Marone F, Stampanoni M, Schmidt V and Wood V 2016 *Nat. Commun.* **27** 12909
[35] Linlin L *et al* 2023 *Journal of Energy Storage* **73** Part D109182
[36] Shanshan W, Qinghai L, Min C, Weihua P, Yulong W and Mingde Y 2016 *Electrochim. Acta* **215** 473–82
[37] González J, Laborda E and Molina Á. 2023 *J. Chem. Educ.* **100** 697–706
[38] Wang S *et al* 2021 *Nat Rev Methods Primers* **1** 41
[39] Duan Q and Chen H 2017 *IOP Conf. Ser.: Mater. Sci. Eng.* **207** 012020
[40] Laghari A J *et al* 2023 *Int. J. Hydrogen Energy* **48** 15447–59